Journal of Nanobiotechnology

RESEARCH Open Access

Nanopore assay for fingerprinting DNA binding and quantifying real-time cleavage by catalytically active Cas9 enzyme

Punitkumar Nagpure[1], Sarangi Suresh[1], Divya Shet[1] and Gautam V. Soni[1*]

Abstract

Nanopore sensing, a high-resolution DNA sequencing technology, is rapidly expanding into novel and exciting directions of probing specific DNA-enzyme interactions. Although proven excellent for the detecting structural features of bare DNA, quantitative measurements on enzyme-DNA complexes and their real-time activity are lagging and only starting to emerge for long DNA templates. Signal-to-noise requirement and high translocation speeds make it difficult to detect protein bound on biologically relevant plasmid-length DNA. To this end we report accurate position detection of a catalytically active Cas9 bound to its single or multiple target sites on the DNA. Protein position is fingerprinted using event charge deficit (ECD) based analysis of the high signal-to-noise electrical signals as the complex translocates through a glass nanopore. Using a time-dependent assay, we quantify the kinetics of the released products upon enzymatic cleavage of the target DNA by the wild-type Cas9 nuclease. Our approach enables the nanopore-based single-molecule sensing of DNA-protein complexes, for real-time monitoring of biochemical reactions. This may help understand protein binding & localization as well as improve Cas9-based targeting in genome engineering applications.

Keywords Nanopore detection, DNA folding, Protein bound DNA, Translocation control, Nanopore enzyme kinetics, Resistive pulse sensing

Introduction

Solid-state nanopore is an emerging single-molecule measurement platform for probing DNA-protein complexes at the molecular scale while providing high throughput detection. Nanopore sensors are a high resolution, label-free detection technique that works on resistive pulse sensing. Biological nanopores are made from pore forming proteins, such as α-hemolysin and MspA, embedded in lipid membrane. On the other hand solid-state nanopores are nanometer-sized holes fabricated in thin solid-state membranes or at the tip of glass nanopipettes [1–8]. The analyte molecule, in electrolyte buffer, electrophoretically translocates through a nanopore under an applied voltage. This causes temporary blockades in nanopore current for the translocation duration. These electrical events form typical nanopore signal, characterized by conductance blockade (ΔG) and translocation time (Δt) which correspond, respectively, to the dimensions and the charge or length of the analyte molecule [1]. Recently, the nanopore platform has been utilized to detect DNA as well as other biological nanostructures [5, 9–16]. There are also recent nanopore studies of DNA-protein complexes that are detected, such as EcoRI, RecA, RNAP, Nuclesomes etc. [6, 17–23]

*Correspondence:
Gautam V. Soni
gvsoni@rri.res.in

Full list of author information is available at the end of the article

Graphical abstract

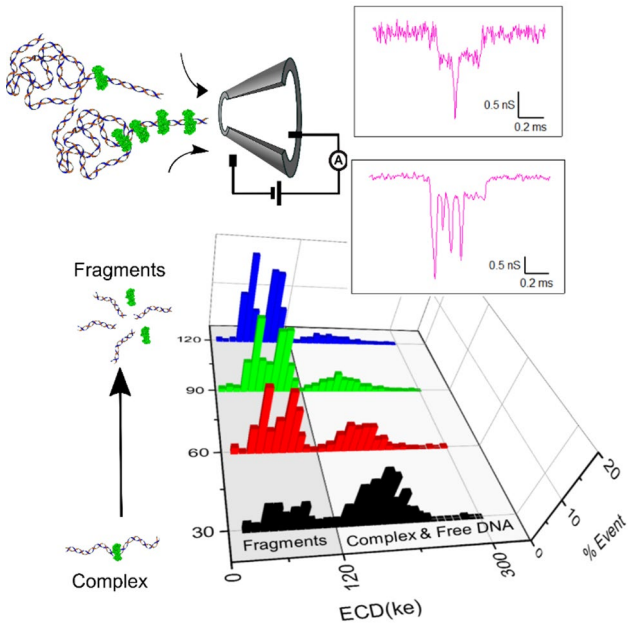

Application of nanopore platform in fingerprinting binding location of protein bound on the DNA, has been a subject of intense research. This utilize basic principle of resistive pulse technique where protein bound DNA molecule is electrophoretically translocated through the nanopore filled with ionic solvent producing additional secondary drop on background DNA level due to bound protein. There has been previous studies that use secondary spike to estimate binding location of proteins including ZEP [24], DNA–antibody complexes [21], RNA polymerase [25], and catalytically inactive Cas9 [26, 27]. These studies typically employed long DNA constructs, such as 20 kb – 48 kb linear DNA as substrates for protein binding. However, these long DNA molecules have a higher tendency to translocate through the nanopore in folded in conformation, which interfere with identification and localisation of protein secondary spike. Additionally, nanopore-based approaches have been used to monitor the cleavage products of Cas12a enzymes, utilizing DNA tetrahedron origami structures or circular single-stranded DNA as carrier molecules for the cleaved fragments [28–30]. More recent work has also demonstrated that polymer-based crowding agents can enhance nanopore sensitivity, enabling the monitoring of cleavage activity at low ionic strength conditions of 0.1 M KCl [31]. However, operating at lower salt concentrations presents several challenges, including non-linear current–voltage relationships, increased interactions between proteins and nanopore walls. Even though recent advancement is excellent for capturing some aspects of the DNA-protein complex, quantifying precise physical properties of the DNA-enzyme system such as protein volume, enzymatic products and rate kinetics remains challenging due to the experimental complexity, chemical treatment of the sample and the required sensitivity.

In this work, we utilize the CRISPR-Cas9 [32, 33] technology to form the DNA-protein complex and demonstrate a detailed event charge deficit (ECD) based analysis to precisely quantify DNA-enzyme interaction. We first establish a complete work plan to accurately quantify different DNA lengths from a mixture using our conical glass nanopore system and a detailed event charge deficit (ECD) based analysis. This allowed us to identify the lengths of the translocating DNA molecule with 189 bp resolution (in a < 2 kbp range). We then show identification of Cas9 complexed DNA molecules translocating through the nanopore, where the Cas9-bound DNA complexes were distinctly identified by the presence of secondary conductance spikes in the nanopore signal. We employ ECD analysis to localize the position of a centrally-located Cas9 enzyme on the DNA with better than 4% error. Owing to our high signal-to-noise, we further demonstrate detection of multiple Cas9 molecules bound to a multi-target DNA. Finally, we apply the ECD-based DNA length analysis to measure real-time product release after cleavage of the target DNA by the catalytically active Cas9 enzyme.

This work expands the high-resolution detection of nanopore platform from DNA sequencing applications to single-molecule enzymatic assays. We envision this as

a first step in many new potential applications of measuring specific and non-specific protein binding and functional enzymatic assays, monitoring assembly and disassembly of multi-protein & DNA complexes.

Materials and methods

Nanopore fabrication and experiment

We used a laser-assisted glass capillary puller (P-2000G, Sutter Instrument) to fabricate glass (quartz) nanopores, as described previously [4, 5]. Briefly, the capillaries (0.65 mm (OD) x 0.35 mm (ID), Sutter Instrument) were pulled with the following two-line program:

Line	HEAT	FIL	VEL	DEL	PUL
1	650	3	45	145	75
2	480	0	25	128	200

This capillary pulling program results in pulled capillaries with nanometer-sized (50–80 nm) pores at their tip. We then shrink these nanopores to desired pore diameters (~20 nm in this study) by irradiating the tips with an electron beam (3 keV) from the Scanning Electron Microscope (SEM, Carl Zeiss Ultraplus FESEM). Final nanopore diameters and taper dimensions of the capillary were quantified by SEM and optical imaging, respectively (see Fig. 1A and individual pore information in Table S10 and Figure S17). Before each experiment these quartz nanopores were cleaned in oxygen plasma using the Plasma Prep-III system (SPI Supplies) to make them hydrophilic and then mounted in a custom-made Teflon fluid cell using Ecoflex 005 glue (Smooth-On Inc.). The fluid cell has two chambers and the capillary with the nanopore was mounted across the two chambers (see schematic in Fig. 1B). The chamber with nanopore mouth (*cis*-chamber) was filled with nanopore buffer (NPB) containing 2 M LiCl in 10 mM Tris-HCl, 1 mM EDTA, with pH 8 and left for 5 min to let the buffer fill the nanopore and its conical taper by capillary action. Then NPB was added into the *trans* chamber filling the back side of the capillary. The fluid cell with the nanopipette was then placed in a desiccator for 10 min to remove

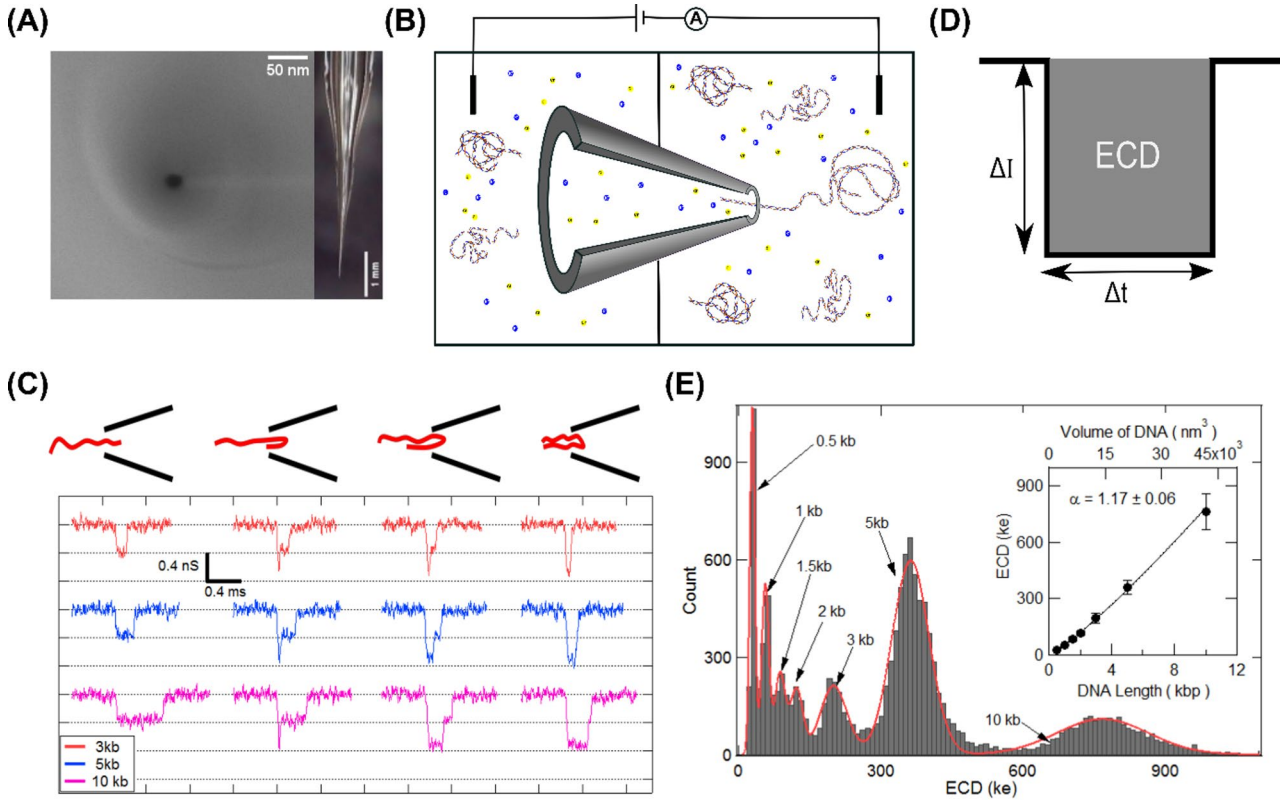

Fig. 1 Detection and characterization of different sizes of linear DNA in glass nanopore. (**A**) Left: SEM image of a typical 20 nm diameter glass nanopore. Right: Optical side-on image of the tapered glass capillary. (**B**) Schematic of the experimental setup showing glass nanopore mounted on Teflon fluid cell along with buffer (yellow and blue ions) solution and sample (DNA). The voltage (500 mV) is applied through Ag-AgCl electrodes and current is measured using the amplifier. (**C**) From the custom-mix of DNA, representative events corresponding to 3,5, & 10 kb DNA translocating through the 20 nm nanopore is shown. Different possible folded configurations corresponding to the events are shown at top. (**D**) Schematic showing typical translocation event parameters of current blockade (ΔI) and the dwell time of the event (Δt). The gray shaded area of the event measures the event charge deficit (ECD). (**E**) ECD histogram from events ($N = 14391$) of custom-mix sample of DNA molecules (sizes range 0.5–10 kb) translocating through 20 nm nanopore. The inset shows the relationship between ECD peak values and volume ($\pi r_{DNA}{}^2 L_{DNA}$) of the translocating DNA molecule. Error bars are standard deviations of the Gaussian fits. The solid line is a power-law fit with exponent $\alpha = 1.17$

any air bubbles. I-V curves and open pore current were recorded to check for linearity and stable low-noise (< 5 pA) baseline behavior before adding the sample. Ag-AgCl electrodes and Axopatch 200B amplifier (Molecular Devices) were used for all current measurements in this work. Typical sample concentrations (to minimize pore blockage) used in translocation experiments are 0.8 nM for free DNA and 0.07–0.14 nM for Cas9-DNA complex. The hardware bandwidth on the amplifier was set to 100 kHz and the data was acquired at a sampling rate of 200 kHz using a NI-PCI 6251 DAQ card. Custom-written LabVIEW (National Instruments) codes were used for data acquisition and further analysis. Current data was low-pass filtered with a 25 kHz cutoff for all event detection and analysis.

DNA sensing and sizing capabilities of our nanopores were tested using our custom-mix DNA sample. This was made by adding 5 and 10 kb linear plasmid DNA to a 1 kb DNA ladder (NEB N3232S). Final concentrations of each DNA length in the custom-mix are shown in Table S1A.

Preparation of target DNA for cas9 binding

The target DNA was pGEM-3z/601 plasmid (3025 bp) with the target sequence as: 5′-GGCACCGGGATTCT CCAGGG-3′. Two distinct positions of the same target sequence were achieved by linearizing the plasmid DNA with two different single-cut restriction enzymes. The plasmid linearized with ScaI-HF (NEB, R3122S) enzyme resulted in a Cas9 target sequence at 1853 bp from the cut end. This target DNA is referred to as "center-target" in the study. Linearization with the restriction enzyme EcoRI-HF (R3101S) resulted in the Cas9 target being at 215 bp from the cut site. This target is referred to as the "edge target" in this study. For multiple Cas9 binding to DNA, we used a 5094 bp linear DNA (linearized from pUC18-12 × 601 plasmid, from the Dekker lab) which has 12 repeats of the same target sequence on one half of the DNA (see Fig. 4A).

Duplex RNA formation

The CRISPR RNA (crRNA) and *trans*-activating CRISPR RNA (tracrRNA), corresponding to the target sequence, were purchased from Integrated DNA Technology (IDT, USA). They were resuspended in nuclease-free buffer (30 mM HEPES, 100 mM potassium acetate, pH 7.5, provided by the manufacturer) to make a 100 µM stock of each RNA. The formation of the duplex RNA was achieved by mixing crRNA and tracrRNA in nuclease-free buffer at an equimolar concentration, resulting in a final duplex guide RNA of 1 µM. The mixture was heated to 90° C for 30 s, then slowly cooled to room temperature (1 h) to yield the crRNA-tracrRNA duplex (RNA).

Cas9-RNA and DNA binding reaction

The Cas9 Nuclease, *S. pyogenes* for the experiments were purchased from New England Biolabs (NEB, M0386S). RNA loaded Cas9 were made by mixing the duplex RNA and Cas9 enzyme in 1:1 molar ratio at 60 nM concentration and incubated for 15 min at 37° C in HEPES buffer (25 mM HEPES-NaOH (pH 8.0), 150 mM NaCl, 1 mM $MgCl_2$). The binding to the target DNA was achieved by adding the target DNA to the RNA loaded Cas9, maintaining the molar ratio of 1:30:30 (DNA: Cas9: RNA) and incubating for 1 h at 37° C. After the reaction, the samples were used immediately. We have previously shown [34] that this reaction results in stable Cas9-DNA complexes.

The stability of the Cas9-DNA complex in NPB (with 2 M LiCl) was verified using an electrophoretic shift assay, as shown in Figure S1. The Cas9-DNA complex was incubated in 2 M (LiCl) salt and tested for complex stability, for up to 2 h. We note, that in the duration of 2 h, the complex band reduces in intensity, gradually (Figure S1 lanes 9–12). This slow release of products, allows for measurement of Cas9-DNA complexed structures within our typical experiment duration (15–45 min). Note that, the release of cleaved products is discussed later in the text (see Fig. 6). The cleaved products could be completely released from the complex by heating the sample to 90° C for 10 min (see Lane 13 in Figure S1).

For the multi Cas9-DNA complex, 5094 bp (5 kb) DNA and RNA-loaded Cas9 were mixed in a 1:40:40 ratio and incubated at 37° C for 1 h and then at 4° C overnight to maximize the binding. This DNA to Cas9 ratio resulted in a sub-saturated number of Cas9 bound to the possible 12 target sites of the 5 kb DNA.

Results

Quantitative nanopore analysis of DNA sizing

First, we demonstrate the sensitivity of our nanopore platform in quantifying linear DNA of different lengths. We used nanopores of size ~ 20 nm in diameter for this study (see Fig. 1A). After adding the DNA mixture into the experimental chamber translocation events were recorded at 500 mV as shown in the schematics of Fig. 1B. Typical example of the baseline current before and after adding the sample are shown in Figure S2. Voltage driven translocation events of individual DNA molecules traversing through the nanopore are detected and for every event, parameters such as the current drop (ΔI) and the duration of translocation time (dwell time, Δt) (see definitions as schematics in Fig. 1D and Figure S2D) are recorded. To uniquely correlate the measured ECD values of the events to the DNA length, we compared ECD values measured for a mixture of DNA lengths (3,5 and 10 kb) with ECD histograms measured for individual DNA lengths. Each peak was assigned a specific DNA

length, by comparing the mixture histogram to those obtained from individual DNA samples (Figure S3A). This allows us to identify various DNA lengths in a sample-mix, also, conversely, isolate events corresponding to a specific DNA length by applying an ECD filter to a mixture of events. In an experiment with DNA mixture, since we can now filter and count the events corresponding to individual DNA lengths, a comparison of event ratio to sample ratio we also establish no length-dependent capture bias across the DNA length range tested in this study (Figure S3B, Table S1B, S3A).

To get a complete dependence of ECDs on DNA length, we next expand our experiment to broader size range DNA length from 0.5 kbp to 10 kbp of custom-mix of linear DNA (see material and methods), with the final concentration of each size of DNA tabulated in Table S1A. A representative selection of the translocation events extracted from custom mix sample is shown in Fig. 1C. We see the multi-level events as seen previously [5] which correspond to unfolded (linear) as well as partially and fully folded conformations of DNA molecules as they translocate through the nanopore. As the number of DNA folds increases (from left to right in Fig. 1C), the conductance decreases in well-defined steps (dotted lines). We also see that the translocation times increase with DNA length.

A quantitative identification of the length of the translocating DNA molecules, irrespective of its conformation, can be done by evaluating its event charge deficit (ECD). The integral of the current drop (ΔI) over the dwell time (Δt) duration for an event is termed as its event charge deficit (see schematic in Fig. 1D). The ECD of each DNA molecule translocating the nanopore is proportional to the volume of ions displaced and independent of the conformation (linear or folded) in which the molecule translocates. In Fig. 1, we used a custom-mix DNA sample of sizes 0.5–10 kb. Each of these DNA lengths translocate through the nanopore (in various conformations) producing events with ECD characteristics corresponding uniquely to their size. We collected more than 10,000 events and evaluated their ECDs (see histogram in Fig. 1E). It shows that the mixture of DNA lengths translocating through the nanopore results in well-separated ECD peaks with the peak values proportional to the respective DNA lengths. The peaks corresponding to specific DNA lengths were identified by correlating relative concentrations of DNA lengths to ECD peak heights. We compared ECD histograms of sample containing DNA lengths (0.5 kbp to 3 kbp) of 1 kbp DNA ladder (see Figure S3C (A & B)) to the custom-mix DNA sample and found new peaks emerging corresponding to the externally added 5 kbp and 10 kbp DNA lengths (see Fig. 1E and Figure S3C (C & D)). Average ECD peak positions (from multiple nanopore and sample concentrations experiments) corresponding to specific DNA lengths were thus identified and plotted in Fig. 1E (inset) (see also Figure S3C (E & F) and Table S2). Note that the DNA lengths with concentrations lower than 0.11 nM result in very low event frequency and hence are not detected as distinct peaks. The ECD versus DNA volume plot was fitted with the power law equation ECD (ke) = $A \times (V_{DNA})^{\alpha}$, where V_{DNA} is the volume of the translocating DNA molecule in nm^3 and A is the fitting parameter [14]. The fitting reveals a power law dependence of the ECD values on the volume of the translocating DNA. This curve can also be used as a calibration to identify lengths of unknown DNA fragments in the sample. We have reproduced these results with multiple nanopores (see Figure S3C), and the corresponding ECD values are shown in Table S2. The mean power-law exponent from multiple experiments (see Table S3B) was found to be $\alpha = 1.17$. Our results show the sensitivity of our nanopore device and ECD analysis in detecting DNA molecules of length down to 0.5 kbp. From the spread of ECD histograms, we could estimate a length resolution of ~ 189 bp for DNA lengths < 2 kbp (see Table S2 & S3B).

Detection of DNA-Cas9 complex

The Cas9 proteins were bound to the linear 3025 bp DNA at the center target position and the stability of the complex in the experimental buffer (NPB – 2 M LiCl) was confirmed by electrophoretic mobility shift assay (see Material and methods and Figure S1). The control DNA (Fig. 2A) and the Cas9-bound DNA (Cas9-DNA complex, Fig. 2D) were translocated through the same nanopore, back-to-back, at 300 mV. Note, due to the net positive charge of the Cas9 protein [26] it is electrophoretically driven in the direction opposite to the net negatively charged DNA (and DNA-Cas9 complex). Thus, in our experimental bias conditions free Cas9 protein do not travel through the nanopore. The events collected for both samples were analyzed and the ΔG and Δt of each event are plotted as scatter plots in Fig. 2B and E, as indicated. Control DNA translocates through the nanopore in linear or folded configuration (see Fig. 1C). The population of events corresponding to the two configurations is seen as two population scatters in Fig. 2B. Representative events of these two types of translocations are shown in Fig. 2C (a) & (b). The mean event depth of linear and folded DNA was measured to be $\Delta G_1 = 0.44 \pm 0.15$ nS and $\Delta G_2 = 0.78 \pm 0.18$ nS, respectively (see Figure S4). We note that DNA in folded conformation results in blockade levels close to twice that of the unfolded DNA. These two configurations cover most of the translocation events in the case of the control DNA sample.

In the same nanopore, translocation of the Cas9-DNA complex was performed (see Fig. 2D). The events collected were analyzed for ΔG and Δt values and are shown

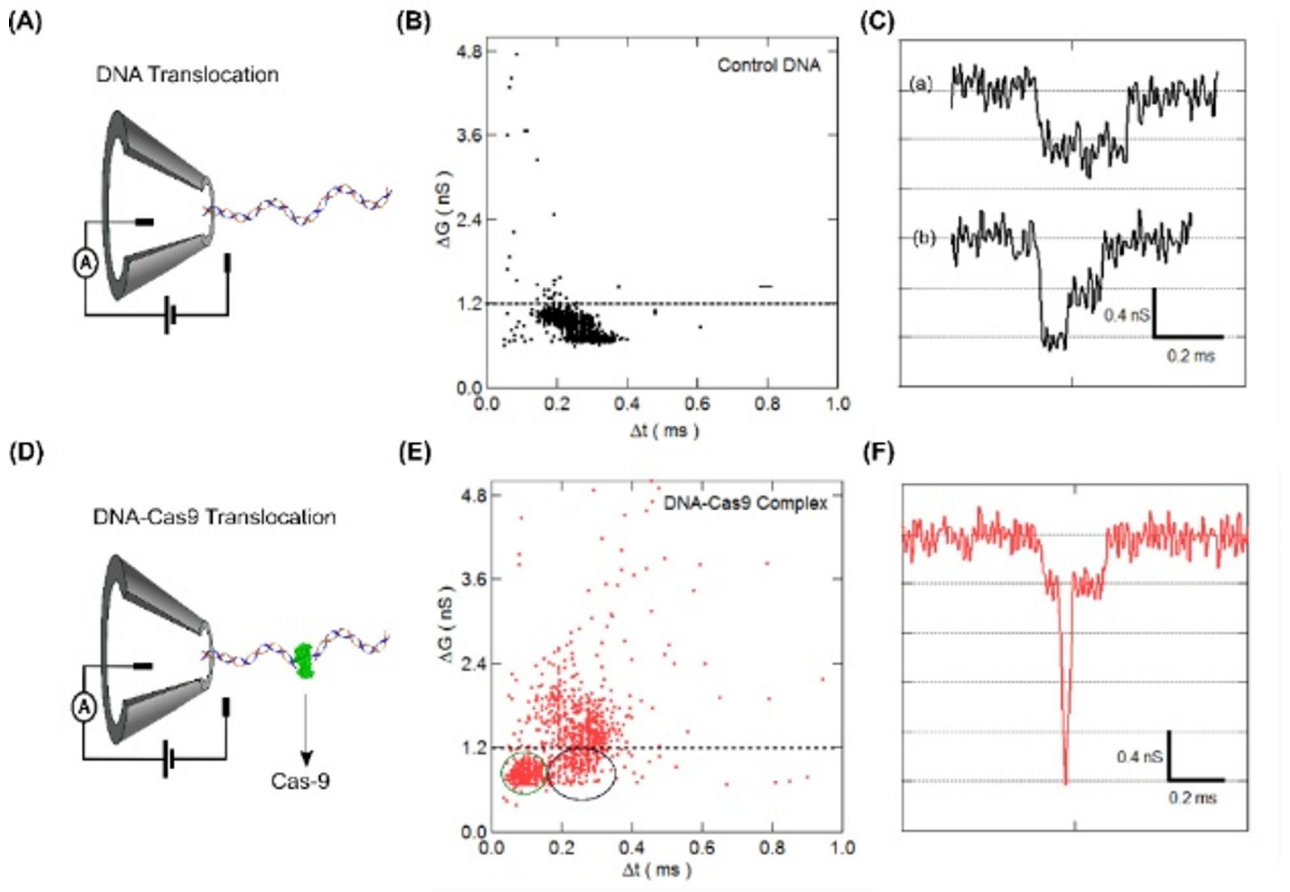

Fig. 2 Detection of Cas9-DNA Complex. (**A**) and (**D**) shows schematics of translocation of control DNA and Cas9-DNA complex through nanopore (300 mV), respectively. (**B**) and (**E**) shows scatter plot of conductance blockade (ΔG) verses dwell time (Δt) for control DNA (*N* = 1567 events) and Cas9-DNA complex sample (*N* = 589 events), respectively. Green and black circles in (**E**) represent cluster of events corresponding to cleaved fragments and unbound DNA respectively. The events above the dotted threshold line represent translocation of stably bound Cas9-DNA complex. (**C**) shows representative translocation event of the control DNA in linear (top, (**a**)) and partially folded (bottom, (**b**)) conformation. (**F**) shows representative event corresponding to translocation of a Cas9-DNA complex. The event shows conductance levels corresponding to the baseline, the DNA and the presence of the Cas9 protein bound on DNA, seen as a distinct spike on top of the DNA level

as scatter plot in Fig. 2E. We note that other than the linear and folded population, the Cas9-DNA complex sample produced a large number of events with very high ΔG values. These events were considered for further analysis. We isolated these events using a simple threshold of $\Delta G > 3 \times \Delta G_{1,}$ as shown in the black dotted line in Fig. 2E. This threshold of ΔG > 1.2 nS was chosen since, for control DNA only 0.05% of the events were found to be above this threshold (see black dotted line in Fig. 2B). These small numbers of events are primarily single-level events with very small dwell times which may be attributed to the translocation of higher-level folding in DNA. Representative of such events is shown in Figure S5. Using this approach, we found that in a typical experiment, about 40–60% of the events are above the threshold during the translocation of the Cas9-DNA complex. This was reproduced for multiple nanopores and sample preparations (see Figure S6 and Table S4). Closer inspection of these events shows a sharp and deep current spike on top of the linear DNA conductance blockade level, as shown in Fig. 2F. We note that these spikes have short duration and a large conductance drop. These events with the secondary spike were exclusively found during the measurement of the Cas9-DNA complex sample. We attribute it to the presence of the Cas9 protein bound to the translocating DNA. A library of such events is shown in Figures S8A & S8B. We observe that the conductance drop due to the Cas9-DNA complex was ~3.4 times the control DNA which is better than previous reports (see Figure S7). [27] Additionally, we observe two distinct populations below the threshold in the scatter plot, Fig. 2E, visually marked with black and green circles. Upon closer inspection, the events marked with a black circle were similar to control DNA events (Fig. 2B), possibly representing the unbound population of control DNA. We also observe a distinct cluster of events with shorter dwell times shown in a

green circle. These events correspond to the translocation of DNA shorter than the target control DNA and are possibly from the translocation of the released cleaved DNA fragments after the Cas9 enzymatic activity. Evaluation of these events by ECD analysis is shown later in the text.

Localization of Cas9 bound on target DNA

Figure 3A (top-left) shows the schematic of the sample where the Cas9 is bound to the target site located towards the center of the linear DNA (see Fig. 3A top-right & Materials and Methods section). This sample is referred to as center-target in the text. Analyzing many

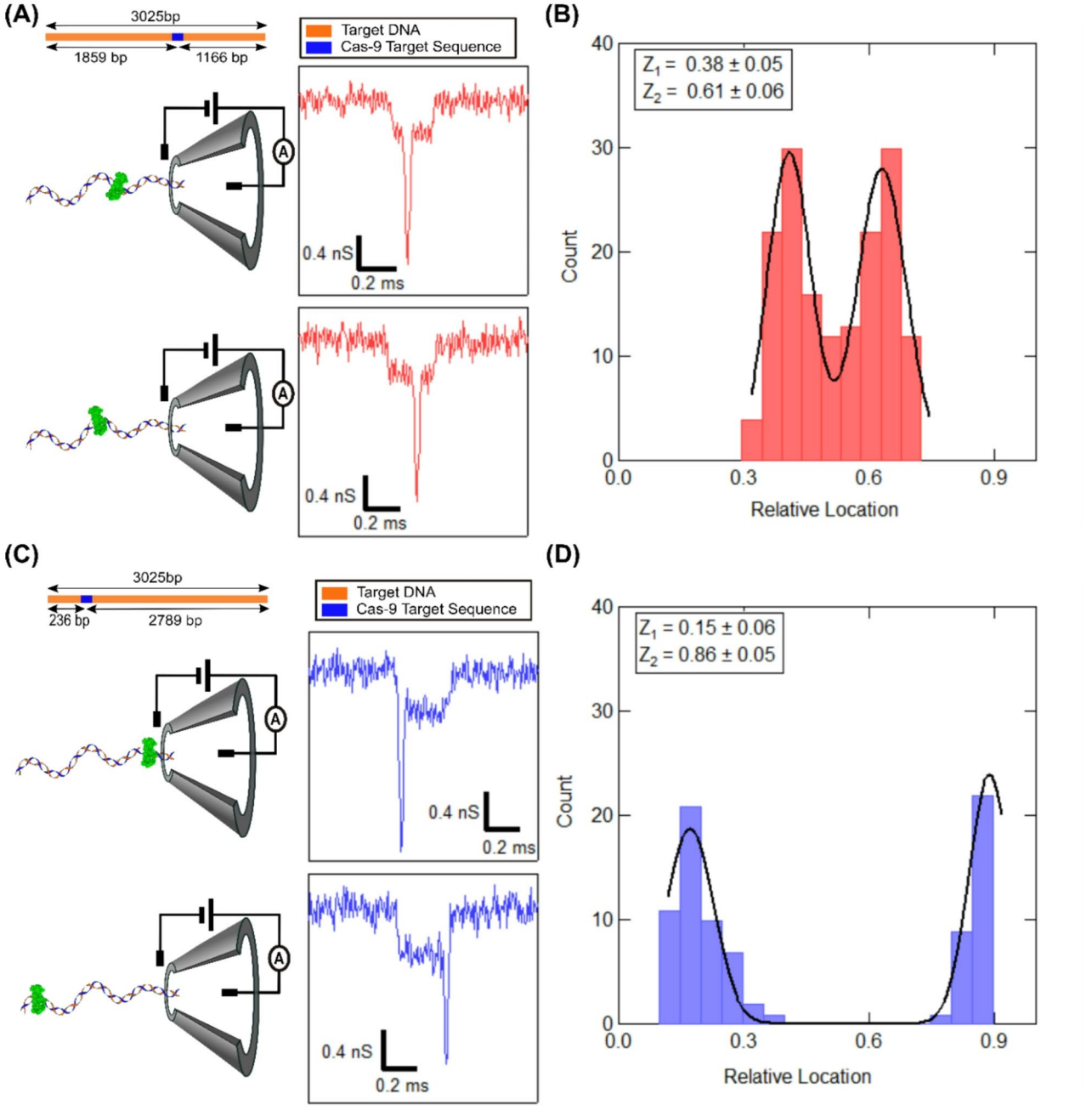

Fig. 3 Spatial localization of Cas9 protein bound to the linear 3 kb target DNA (**A)** (top) shows the position of the target (blue) on the 3 kb DNA (orange), in the case of center-target. Lengths of the target DNA and the cleaved products are indicated. (Bottom) shows schematic (left) and representative event (right) depicting the two orientation in which the complex can translocate through the nanopore (at applied voltage of 300 mV). **(B)** shows a histogram of ECD-based estimation of the spike positions relative to the event length for the center-target sample. (**C)** and (**D**) are the same as above for the DNA-Cas9 complex bound on the edge target. Z_1 and Z_2 are the peak positions that gives an estimate of the relative position of the spike along the DNA event, where the DNA is translocating in the two different orientations

such events with the protein spike, we find that all events have the spike located at two distinct locations along the event. Representative events of these two spike positions are shown in Fig. 3A (right) and Figure S8B. We understand the two protein positions are a result of the Cas9-DNA complex entering the nanopore in two different orientations (as shown in Fig. 3A (left)). This results in the two possible protein positions measured on the translocating DNA.

To further investigate the readout of protein position on DNA from the spike position in the translocation event, we prepared a new Cas9-DNA complex with its target location shifted to the edge (215 bp from the start of the DNA) of the linear DNA (see schematic in Fig. 3C). This sample is called edge-target in the text. The sample with edge target was measured on the same nanopore (as the center-target sample), and the events are shown in Fig. 3C (right) and Figure S8D. Here we again see the bound protein as conductance spikes on top of the DNA blockade events. However, the location of the protein spike is now moved either to the beginning or the end of the event length. These two states again demonstrate that the protein carrying DNA may enter the nanopore in either orientation, which brings the protein at either the start or the end of the event. Note, the protein spikes are also present for Cas9-bound DNA molecules that translocate in (partially or fully) folded conformation. Some of the representative events are shown in Figure S9 and S10 (see also Table S4).

We analyze the events with well-defined protein spikes to localize the physical position of the protein on the DNA. We employ our, previously established, ECD-based analysis method to correlate the position of electrical spikes found in translocation events to the actual location of Cas9 protein bound on the linearly translocating DNA [5]. Note that for this analysis, only those events are considered where the DNA was translocated in an unfolded configuration. This was done to eliminate challenges brought in by events with spikes on folded or partially folded DNA. We calculated the relative location of the Cas9 spike by taking a ratio of the ECD up to the center of the protein spike to the total ECD of the event, as shown below:

$$\text{Relative location of Protein on DNA} = \frac{\text{ECD up to center of protein spike}}{\text{Total ECD of Event}}$$

Spike location, relative to the DNA event (event length scaled to 1) was calculated using the above expression for each event. Figure 3B shows the histogram of identified spike locations relative to DNA length, for the center-target sample. The two distinct peak positions (corresponding to the two entry orientations) were found to be 0.38 ± 0.05 and 0.61 ± 0.06. This result was reproduced on multiple nanopores and sample preparations, as seen in Table S5. From our experiments, the average value of the protein positions for the center-target sample, was found to be 0.4 ± 0.01 and 0.59 ± 0.01, respectively. Our results show excellent agreement with true protein positions (0.39 and 0.61, see Fig. 3A) of Cas9 bound to its targets with < 4% error (see Table S5).

We reproduce the same analysis for the edge-target sample. Figure 3D shows the histogram of the protein spike positions measured in translocation data. We find that the mean values of peak location were found to be at 0.15 ± 0.06 and 0.86 ± 0.05, corresponding to the two orientations the protein-DNA complex enters the nanopore. This is also repeated on multiple nanopores, as shown in Table S5 and Figure S11. The mean values of the relative protein location were estimated to be 0.17 ± 0.05 and 0.85 ± 0.03, respectively. The true values of the relative location for the edge-target sample were calculated to be 0.08 and 0.92. In the case of the edge target sample, the protein location is at the very edge of the DNA. The observed deviation in measured protein location, in this case, is possibly due to large velocity fluctuation at the entry and exit of translocation as reported earlier [35–37]. From Fig. 3B and D, we also note that the probability for entry of either end of the DNA into the nanopore was similar in both center and edge-target samples. This suggests that the Cas9-bound DNA molecule randomly selects, from the well-equilibrated ensemble of both orientations, any one end to enter into the nanopore, as reported earlier [38].

The ECD of the protein spikes in the translocation events also allows us to estimate the hydrodynamic volume of the Cas9 protein. First, we extracted the protein spike for every event with a custom-written LabVIEW code and calculated its translocation characteristics, such as its ΔG, Δt and the ECD (see Figure S7 & Table S6). The power law dependence of ECD on the volume of the translocating molecule was measured earlier in Fig. 1E (inset). By using the volume of the 3 kb DNA, measured on the same nanopore, as in-situ control, we estimate the volume of Cas9 protein from multiple nanopores (see Table S6). From our experiments, the average volume of the Cas9 protein was found to be 3336.1 ± 388 nm^3. Our measured protein volume agrees with the literature [33] value of 3057.6 nm^3, with less than 10% error (see Table S6).

Detection of DNA-Cas9 multi-protein complex

Next, we expand the application of our method to demonstrate the detection of multiple Cas9 proteins bound onto the same DNA molecule. For this experiment we used 5094 bp (~5 kb) linear DNA with 12 repeats of the 200 bp region with one Cas9 target per region. The

Cas9 target is located 35 bp from the beginning of each 200 bp region. A schematic of the DNA with multiple target sites is shown in Fig. 4A (right). In this experiment, we optimized the DNA and crRNA loaded Cas9 protein ratio to create sub-saturated (3–5 Cas9 protein per DNA) binding of Cas9 on the 12 target sequences. This ratio was optimized to ensure clear identification of multi-peaks during translocation signifying multiple proteins bound on the DNA. This was found to be essential for the reproducibility of the results (as higher concentrations of protein would clog the nanopore prematurely) as well. The multi-Cas9-DNA complex molecules were translocated through the 20 nm nanopore at 300 mV. A collection of representative events showing the translocation signal for the sample is shown in Fig. 4B and C. The events show DNA translocation with multiple protein spikes distributed along the DNA level. We attribute these spikes to multiple Cas9 bound to target DNA, since

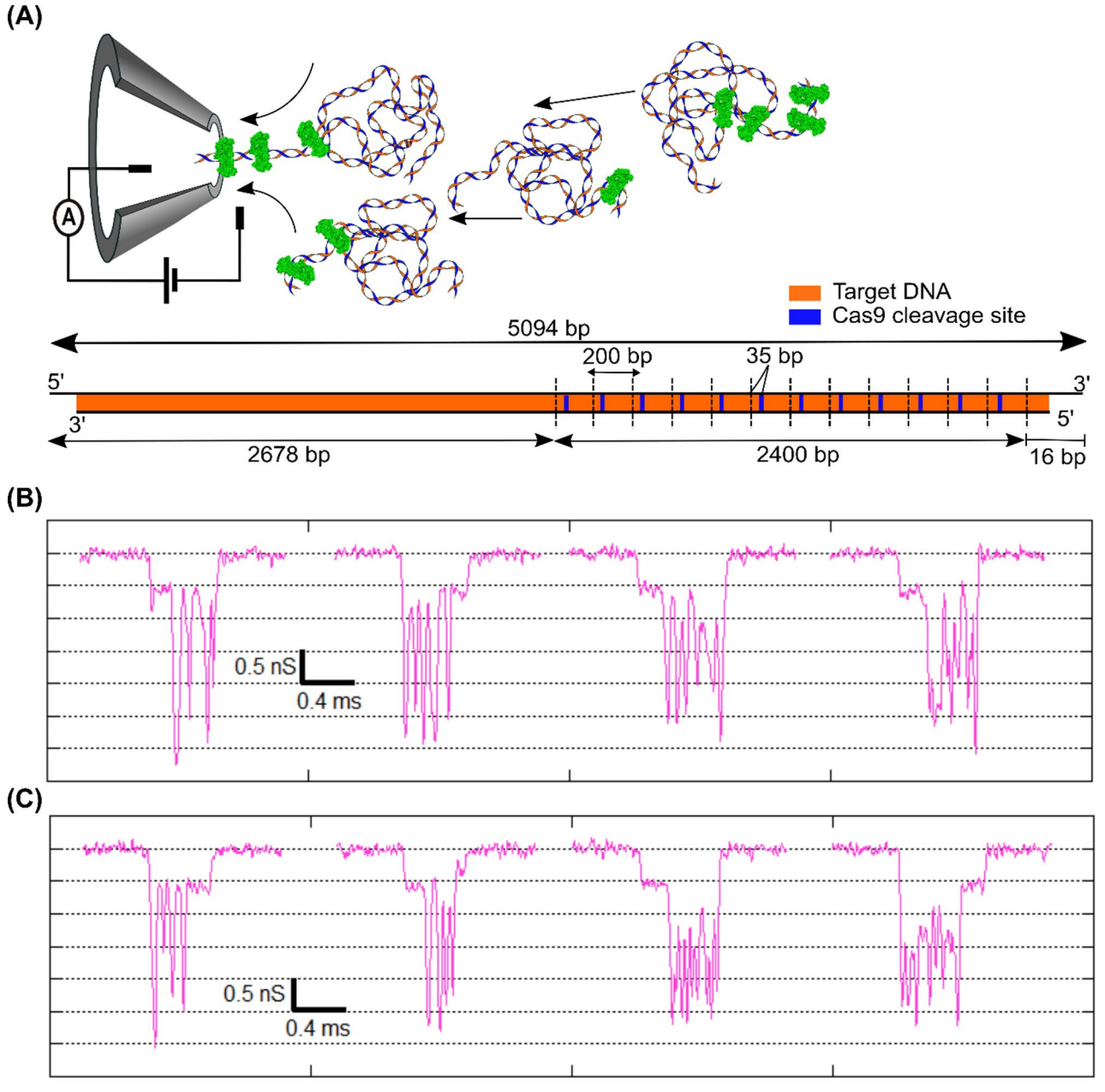

Fig. 4 Detection of complex with multiple Cas9 bound to the DNA. (**A**) Schematic of the multi-Cas9 bound DNA sample and the translocation process through the nanopore at 300 mV. Multiple Cas9 protein bound on DNA is shown in green. (Bottom) shows the 5094 bp DNA (5 kb, in orange) with 12 repeats of 200 bp region (dotted vertical lines), each carrying a Cas9 target site shown in blue. In our experimental conditions, Cas9 to DNA ratio is chosen such that sub-saturated (3–5 Cas9 bound per DNA) arrays are formed. (**B**) and (**C**) show a library of representative events demonstrating multiple Cas9 protein bound on the DNA being detected as multiple spikes in events recorded during translocation of individual complex molecules

they have similar characteristics as shown with single Cas9-DNA complexes (see Fig. 2F). Since the targets are located on one side of the DNA and the translocation could happen in either orientation, we find that the protein spikes were distributed randomly at either the start or end of the event, as can be seen in Fig. 4B and C. In multiple repeats of our experiments, we observe 20–25% of events to be over the ΔG threshold (see Fig. 2E) that correspond to Cas9-DNA complexes, of which 50–70% of events show two or more spikes per event. We observed a variety of events with anywhere between 1 and 6 protein spikes. A library of such events is shown in Figure S12. In addition to the unfolded events, Cas9-DNA complex molecules can translocate in folded conformation producing complicated event structures. Some of such representative events are shown in Figure S13A & S13B. These results and event characteristics were reproduced on different nanopores as tabulated in Table S7. We further quantified total event ECD with increasing number of secondary spike and we expect increase in the total event ECD with higher number of bound proteins. The Figure S13C shows mean event ECDs for events with increasing number of protein spikes. We observe the mean ECD increases systematically with the number of secondary spikes, confirming that the number of spikes corresponds to the number of Cas9 proteins bound.

Importantly, we note that binding of multiple Cas9 proteins on the DNA, seems to slow down translocation. This is from the observation (Fig. 4B and C) that the region with protein spikes seems to have longer translocation times when compared to the translocation time of the equally sized bare DNA. This slowing down of the molecule (in the nanopore) could either be due to the altered charged state of the DNA-protein complexes or due to increased wall interactions. This is interesting and will be followed up on in a future publication. As a result of the variable translocation speed of protein-bound DNA in the nanopore, we can detect and count the bound protein molecules, but their exact positions along the DNA remain uncertain.

Characterization of the enzymatic activity of catalytically active Cas9

We next apply the robust nature of the ECD-based analysis, to quantify the enzymatic activity of the wild-type DNA-binding enzyme, Cas9. It is shown earlier that the wild-type Cas9 enzyme remains stably bound to its target DNA until the cleaved products are released upon exposure to agents, such as salt, temperature, or detergent[34]. We quantify time-dependent release of the cleaved products to measure the temporal stability of the catalytically active Cas9 enzyme on the target DNA, in our experimental conditions.

To measure the constituents of our Cas9-DNA complex sample, we calculated the ECD of every collected event. A schematic of this experiment is shown in Fig. 5A. The histogram of the estimated ECD values is shown in Fig. 5C (top). We find four distinct peaks in the ECD histogram, which should correspond to four distinct populations. Gaussian fitting of the four peaks reveals the mean values as $ECD_1 = 59.46 \pm 9.46$ (ke), $ECD_2 = 106 \pm 10.65$ (ke), $ECD_3 = 184.16 \pm 12.95$ (ke) and $ECD_4 = 239.39 \pm 49.44$ (ke). These values are also shown as vertical dotted lines for visual clarity.

To confirm the identities of our ECD peaks, we re-measured the translocation of the same sample, after heat-release of the products, in the same nanopore. The heat treatment of the Cas9-DNA complex sample at 90° C for 10 min denatures the Cas9 protein, resulting in complete release of the cleaved fragments (see Fig. 5B and Figure S1 (lane 13 in (A)). In the ECD histogram of the heat-treated sample, we observe only three distinct peaks (see Fig. 5C (Bottom)). Comparing the locations of the peaks in the two histograms (Fig. 5C (top & bottom)), we find that the population with the largest ECD value (population (iv)) is absent, whereas the other three peaks remain as is. This confirms our annotation of the population marked (iv) to be the Cas9-bound DNA complex and population (iii) as the Cas9-free target DNA. Consequently, the peaks (i) and (ii) are identified to be the populations corresponding to the two cleaved fragments that are released after Cas9 cleavage of the target DNA. Note, ECD histograms of the translocation of the control DNA sample do not show multiple peaks (see Figure S15). These results were reproduced in multiple nanopores and multiple sample preparations (see Figure S14 and Table S8).

We quantify the length of the released DNA fragments (population (i) and (ii)), from the ECD peak values using the power law dependence established earlier in Fig. 1E inset. Using the ECD value of the free DNA (3 kb) (shown in Fig. 5C (bottom)) as the in situ control, we estimate the DNA lengths of the populations (i) and (ii) using the expression $\frac{ECD_{fragment}}{ECD_{control}} = \left(\frac{V_{fragment}}{V_{control}}\right)^{\alpha} = \left(\frac{L_{fragment}}{L_{control}}\right)^{\alpha}$. From the above calculations the lengths of the DNA fragments in populations (i) and (ii) were estimated to be 1122 ± 123 bp and 1826 ± 197 bp respectively. The expected values of the two fragments are 1166 bp and 1859 bp. Our estimated DNA fragment length values, measured in multiple nanopores, agree with the expected fragment lengths within 4% error (see Table S8B).

This allows us to demonstrate, for the first time, simultaneous detection and quantification of enzyme-bound, enzyme-free and enzymatically cleaved product populations, in the nanopore platform.

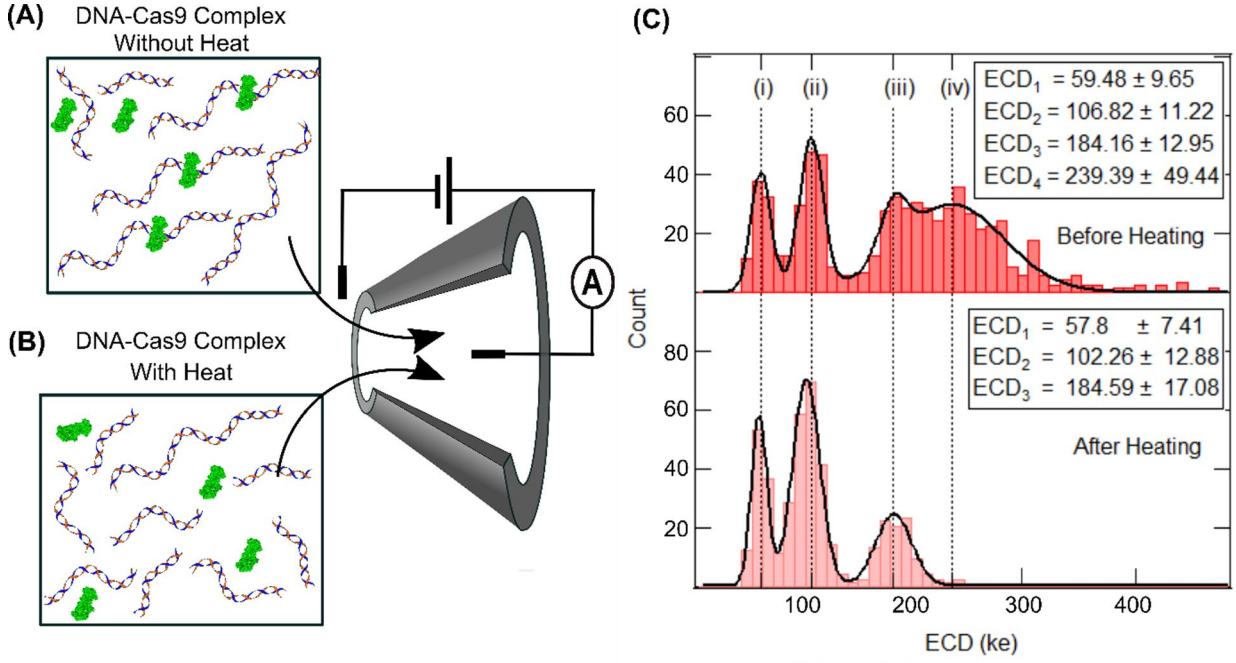

Fig. 5 Detection of Cas9-bound and Cas9-cleaved DNA. (**A**) shows a cartoon of a Cas9-DNA complex sample at room temperature. The reaction mix contains free DNA, free Cas9 protein, Cas9-bound DNA and Cas9-cleaved DNA fragments. (**B**) shows a cartoon of the Cas9-DNA complex sample after heat-release of products. The sample contains denatured Cas9 protein, released cleaved DNA products and free DNA. Both samples are measured using the same nanopore at 300 mV, back-to-back, as shown in the middle schematic. (**C**) shows ECD histograms of the two, room temperature (top) and heat-released (bottom), samples. Histograms show populations for Cas9-bound DNA (iv), free DNA (iii), and the two Cas9-cleaved products (ii) and (i), as distinct ECD peaks. Note the absence of the Cas9-bound DNA peak in the heat-released sample

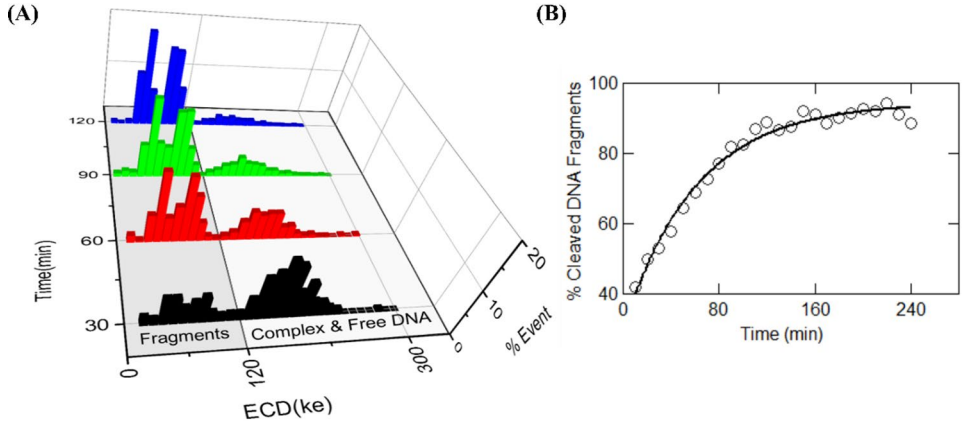

Fig. 6 Real-time release of cleaved products by catalytically active wild-type Cas9 protein. (**A**) Quantifies different populations of DNA fragments that are released by Cas9 cleavage at room temperature. Events are accumulated for 30-min time intervals and shown at time points of 30, 60, 120 and 180 min (measured at 500 mV). Note the decrease in Cas9-bound DNA population and increase in the cleaved DNA fragments population with time. The percentage of cleaved fragments was calculated from the number of events under the ECD histograms (shaded region in (**A**)) collected for each 10 min interval and is plotted in (**B**). The solid line shows a fit to a first-order rate equation with a rate constant of $0.017 \pm 0.0013\ \text{min}^{-1}$

The above quantification of the components of a DNA-protein reaction mixture also allows us to measure the temporal progression of Cas9-based cleavage of the target DNA. For this experiment, we continuously recorded the translocation events of the Cas9-DNA complex sample through the nanopore (at 500 mV), for up to 4 h. At different time points, we quantified relative fractions of the cleaved products using the population identification strategy developed by ECD analysis. Figure 6A shows ECD histograms of events collected at four different time points. It shows peaks corresponding to the two cleaved fragments (shaded region) and the population corresponding to the free and Cas9-bound DNA (unshaded region). Note that due to very small ECD differences between the third and the fourth peaks, they are sometimes indistinguishable. The two peaks corresponding to

the cleaved fragments are, however, always resolvable and the number of events in these two peaks increases with time, with a corresponding decrease in the higher ECD peaks. This indicates time-dependent release of cleaved products from the Cas9-bound DNA complexes. We calculated the percentage of cleaved products, by counting the number of events under the cleaved products ECD peaks, at every 10-minute interval and showing this progression in Fig. 6B. The percentage of cleaved fragments increased exponentially with time and saturated after about 180 min. We fitted the first-order rate equation to the data in Fig. 6B and found the rate of release of the cleaved products to be 0.017 ± 0.0013 min^{-1}. Our nanopore based measurement of rate kinetics for the release fragments were reproduced in multiple nanopore and are in good agreement with previously reported values in the literature [39, 40]. We also found that the product release rates are intrinsic to the Cas9 enzyme and are independent of the voltage applied across the nanopore (see Figure S16A and Table S9). We further validate our result by measuring the Cas9 product release kinetics at a different salt concentration (3 M LiCl). We observe faster rate of release of the cleaved fragments in higher salt condition, as expected. This result was reproduced in two different nanopore shown in Figure S16B.

Conclusion

In this work we have presented a nanopore-based assay to localize Cas9 bound at different locations on the target DNA. We show that the Cas9-bound DNA molecules can be uniquely identified from the unbound background by a high-resolution secondary conductance spike during the translocation event of the complexed molecule. A detailed ECD-based analysis was employed to identify the location of the centrally-bound Cas9 protein on the DNA within 4% error. This analysis also allowed us to quantify the volume of the bound protein within 10% of the literature value. For the Cas9-DNA complex, an excellent correlation of the location of the conductance spikes in the translocation events to the physical location of the protein on the DNA was established for Cas9 positioned at multiple places. We employed this detection scheme on DNA complexed with multiple (1–6) Cas9 proteins, which showed corresponding multi-peaks in the translocation events and allowed us to count the number of bound proteins. Although the data in Fig. 3 and Table S5 establishes our accuracy of localization (mean position within 4% (30 bp) with a relative spread of 0.01 (~60.5 bp)) of protein position, the resolution (distinctly localizing two nearby bound proteins) of our system would depend on multiple other factors, including nanopore noise, measurement bandwidth, velocity variations due to protein charge, pore length and geometry. This will be the focus of a future publication. Finally, we showed the quantification of cleaved and released products of the catalytically active Cas9. The unique sizes of the product fragments were quantified using their unique ECD signatures, and the fragment lengths were quantified within 4% error. We also show quantification of the rate of product release, with time, by the enzyme (in our experimental conditions). We find the release rate of Cas9 cleaved products to be 0.017 ± 0.0013 min^{-1}. The experimental result presented has potential application for glass nanopores in Cas9-based targeting in genome engineering applications.

In conclusion, we have developed, through a range of experiments, a nanopore assay to fingerprint location as well as monitor functional activity of enzymes, such as endonucleases, restriction enzymes or any other DNA-binding operator protein, with single-molecule resolution. Our nanopore sensor distinguishes template DNA when translocating bare, as compared to when an enzyme molecule is bound to it. On a 3 kb template DNA we targeted the binding of the Cas9 enzyme using crRNA. Nanopore events for bare DNA, with conductance level corresponding to DNA translocation, could be isolated from the events for the enzyme-bound DNA solely based on the high-amplitude secondary spike in conductance on top of the DNA level. These secondary spikes were shown to be due to the enzyme bound onto the DNA. We showed that the relative location of the spike in the event corresponds to the relative location of the enzyme on the DNA. This fingerprinting of protein location was further confirmed by targeting the Cas9 protein to a 2nd location and measuring the corresponding shift in the relative spike location. We show that ECD-based analysis is a powerful technique to quantify protein position as well as protein volume from these protein spikes. In the case of the multi-proteins bound on DNA, we show high-resolution detection and count of the protein bound on the DNA and show variability in translocation speeds of multi-protein bound region compared to the bare DNA backbone. Importantly, the ECD-based assay presented here allowed us to directly measure, in real-time, the catalytic output of DNA fragments resulting from active Cas9 cleavage. Although there are conventional techniques, like gel electrophoresis, that maybe used to detect protein bound DNA, they require specific DNA staining (radioactive or fluorescent) and have very low resolution for longer DNA. Techniques like TIRF and DNA PAINT would suffer from optical resolution limits whereas the super resolution microscopies can decipher individual molecules but are prohibitively expensive. In contrast, our nanopore assay extracts real-time kinetics directly from continuous single-molecule measurements and achieves higher throughput than other single-molecule techniques. It also enables higher spatial and temporal resolution, as well as multi-species detection, for example

of Cas9-bound DNA, free DNA and cleaved fragments. Information on the location of the bound protein is an additional advantage. Put together, these capabilities make the presented nanopore approach more suitable to decipher an accurate and mechanistic view of protein-DNA kinetics. This combination of high signal-to-noise combined with ECD analysis of events, resulting in real-time analytical quantitation of enzyme reaction output, opens up the field to study DNA and/or RNA specific binding proteins, protein complexes bound to DNA, as well as chromatin structure.

Supplementary Information

The online version contains supplementary material available at https://doi.org/10.1186/s12951-025-03837-6.

Supplementary Material 1.

Acknowledgements
We acknowledge RRI's internal funding and assistance from Mr. Yatheendran & RRI SEM facility in this work.

Author contributions
GVS, and PN conceived the project. PN & GVS planned the experimental protocol. DS & PN contributed in sample preparation. PN and SS performed experiments. PN, SS and GVS performed data analysis. All authors contributed in manuscript writing.

Funding
We acknowledge RRI's internal funding for the project.

Data availability
All relevant data is included in this article.

Declarations

Ethics approval and consent to participate
Not Applicable.

Consent for publication
All authors have provided consent for the manuscript to be published.

Competing interests
The authors declare no competing interests.

Supporting information
Supplementary Information file contains gel images for sample preparation and characterization, characterization of nanopores, control datasets of ECD analysis, and S/N characterization of protein position. Additional details for nanopore experiments, such as complete datasets supporting what is shown in the manuscript, Library of events with single & multiple protein spikes, and reproducibility of nanopore experiments on multiple. Contains supplementary figures (S1-S17) and tables (S1-S10) as mentioned in the text.

Author details
[1]Raman Research Institute, Bangalore 560080, India

Received: 15 August 2025 / Accepted: 4 November 2025
Published online: 21 November 2025

References

1. Wanunu M. Nanopores: a journey towards DNA sequencing. Phys Life Rev. 2012;9(2):125–58. https://doi.org/10.1016/j.plrev.2012.05.010.
2. Albrecht T. Single-molecule analysis with solid-state nanopores. Annu Rev Anal Chem. 2019;12(1):371. https://doi.org/10.1146/annurev-anchem-061417-125903.
3. Wanunu M, Soni GV, Meller A. (2009). Single-Molecule Studies of Nucleic Acid Interactions Using Nanopores. In: Hinterdorfer, P., Oijen, A, editors Handbook of Single-Molecule Biophysics. *Springer, New York*, NY. https://doi.org/10.1007/978-0-387-76497-9_10
4. Bafna JA, Soni GV. Fabrication of Low Noise Borosilicate Glass Nanopores for Single Molecule Sensing. Wanunu M, ed. *PLOS ONE*. 2016;11(6):e0157399. https://doi.org/10.1371/journal.pone.0157399
5. Maheshwaram SK, Sreenivasa K, Soni GV. Fingerprinting branches on supercoiled plasmid DNA using quartz nanocapillaries. Nanoscale. 2021;13(1):320–31. https://doi.org/10.1039/D0NR06219G.
6. Maheshwaram SK, Shet D, David SR, Lakshminarayana MB, Soni GV. Nanopore sensing of DNA–histone complexes on nucleosome arrays. ACS Sens. 2022;7(12):3876–84. https://doi.org/10.1021/acssensors.2c01865.
7. Xue L, Yamazaki H, Ren R, Wanunu M, Ivanov AP, Edel JB. Solid-state nanopore sensors. Nat Rev Mater. 2020;5(12):931–51. https://doi.org/10.1038/s41578-020-0229-6.
8. Muthukumar M, Plesa C, Dekker C. Single-molecule sensing with nanopores. Phys Today. 2015;68(8):40–6. https://doi.org/10.1063/PT.3.2881.
9. Ying YL, Hu ZL, Zhang S, et al. Nanopore-based technologies beyond DNA sequencing. Nat Nanotechnol. 2022;17:1136–46. https://doi.org/10.1038/s41565-022-01193-2.
10. Varongchayakul N, Song J, Meller A, Grinstaff MW. Single-molecule protein sensing in a nanopore: a tutorial. Chem Soc Rev. 2018;47(23):8512–24. https://doi.org/10.1039/C8CS00106E.
11. Platnich CM, Earle MK, Keyser UF. Chemical annealing restructures RNA for nanopore detection. J Am Chem Soc. 2024;146(19):12919–24. https://doi.org/10.1021/jacs.4c03753.
12. Bandara YMNDY, Freedman KJ. Enhanced signal to noise ratio enables high bandwidth nanopore recordings and molecular weight profiling of proteins. ACS Nano. 2022;16(9):14111–20. https://doi.org/10.1021/acsnano.2c04046.
13. Gao T, Gao X, Xu C, et al. Label-free resistance cytometry at the orifice of a nanopipette. Anal Chem. 2021;93(5):2942–9. https://doi.org/10.1021/acs.analchem.0c04585.
14. Fologea D, Brandin E, Uplinger J, Branton D, Li J. DNA conformation and base number simultaneously determined in a nanopore. Electrophoresis. 2007;28(18):3186–92. https://doi.org/10.1002/elps.200700047.
15. Bandara YMNDY, Freedman KJ. Lithium chloride effects field-induced protein unfolding and the transport energetics inside a nanopipette. J Am Chem Soc. 2024;146(5):3171–85. https://doi.org/10.1021/jacs.3c11044.
16. Chen K, Yu R, Zhong C, et al. Electrochemical monitoring of real-time vesicle dynamics induced by Tau in a confined nanopipette. Angew Chem Int Ed. 2024;63(39):e202406677. https://doi.org/10.1002/anie.202406677.
17. Smeets RMM, Kowalczyk SW, Hall AR, Dekker NH, Dekker C. Translocation of RecA-coated double-stranded DNA through solid-state nanopores. Nano Lett. 2009;9(9):3089–95. https://doi.org/10.1021/nl803189k.
18. Raillon C, Cousin P, Traversi F, Garcia-Cordero E, Hernandez N, Radenovic A. Nanopore detection of single molecule RNAP–DNA transcription complex. Nano Lett. 2012;12(3):1157–64. https://doi.org/10.1021/nl3002827.
19. Soni GV, Dekker C. Detection of nucleosomal substructures using solid-state nanopores. Nano Lett. 2012;12(6):3180–6. https://doi.org/10.1021/nl301163m.
20. Ivankin A, Carson S, Kinney SRM, Wanunu M, Fast. Label-Free force spectroscopy of Histone–DNA interactions in individual nucleosomes using nanopores. J Am Chem Soc. 2013;135(41):15350–2. https://doi.org/10.1021/ja408354s.
21. Plesa C, Ruitenberg JW, Witteveen MJ, Dekker C. Detection of individual proteins bound along DNA using solid-state nanopores. Nano Lett. 2015;15(5):3153–8. https://doi.org/10.1021/acs.nanolett.5b00249.
22. Squires A, Atas E, Meller A. Nanopore sensing of individual transcription factors bound to DNA. Sci Rep. 2015;5(1):11643. https://doi.org/10.1038/srep11643.
23. Nuttall P, Lee K, Ciccarella P, et al. Single-molecule studies of unlabeled full-length p53 protein binding to DNA. J Phys Chem B. 2016;120(9):2106–14. https://doi.org/10.1021/acs.jpcb.5b11076.
24. Yu JS, Lim MC, Huynh DTN, et al. Identifying the location of a single protein along the DNA strand using solid-state nanopores. ACS Nano. 2015;9(5):5289–98. https://doi.org/10.1021/acsnano.5b00784.

25. Kaur H, Nandivada S, Acharjee MC, McNabb DS, Li J. Estimating RNA polymerase protein binding sites on λ DNA using solid-state nanopores. ACS Sens. 2019;4(1):100–9. https://doi.org/10.1021/acssensors.8b00976.
26. Yang W, Restrepo-Pérez L, Bengtson M, et al. Detection of CRISPR-dCas9 on DNA with solid-state nanopores. Nano Lett. 2018;18(10):6469–74. https://doi.org/10.1021/acs.nanolett.8b02968.
27. Weckman NE, Ermann N, Gutierrez R, et al. Multiplexed DNA identification using site specific dCas9 barcodes and nanopore sensing. ACS Sens. 2019;4(8):2065–72. https://doi.org/10.1021/acssensors.9b00686.
28. Zhang S, Liu M, Cui H, et al. Detection of small-sized DNA fragments in a glassy nanopore by utilization of CRISPR-Cas12a as a converter system. Analyst. 2022;147(5):905–14. https://doi.org/10.1039/D1AN02313F.
29. Wang J, Luo L, Li Y, et al. A signal on–off strategy based on the digestion of DNA cubes assisted by the CRISPR–Cas12a system for ultrasensitive HBV detection in solid-state nanopores. Analyst. 2022;147(24):5623–32. https://doi.org/10.1039/D2AN01402E.
30. Nouri R, Jiang Y, et al. Detection of SARS-CoV-2 with solid-state CRISPR-Cas12a-assisted nanopores. Nano Lett. 2021;21(19):8393–400. https://doi.org/10.1021/acs.nanolett.1c02974.
31. Chalmers CC, Chau NE, Weckman, et al. Solid-State nanopore Real-Time assay for monitoring Cas9 endonuclease reactivity. ACS Nano. 2025;19(3):3839–51. https://doi.org/10.1021/acsnano.4c15173.
32. Jiang F, Doudna JA. CRISPR–Cas9 structures and mechanisms. Annu Rev Biophys. 2017;46(1):505–29. https://doi.org/10.1146/annurev-biophys-062215-010822.
33. Jinek M, Jiang F, Taylor DW, et al. Structures of Cas9 endonucleases reveal RNA-mediated conformational activation. Science. 2014;343(6176):1247997. https://doi.org/10.1126/science.1247997.
34. David SR, Maheshwaram SK, Shet D, Lakshminarayana MB, Soni GV. Temperature dependent in vitro binding and release of target DNA by Cas9 enzyme. Sci Rep. 2022;12(1):15243. https://doi.org/10.1038/s41598-022-19485-x.
35. Lu B, Albertorio F, Hoogerheide DP, Golovchenko JA. Origins and consequences of velocity fluctuations during DNA passage through a nanopore. Biophys J. 2011;101(1):70–9. https://doi.org/10.1016/j.bpj.2011.05.034.
36. Plesa C, Van Loo N, Ketterer P, Dietz H, Dekker C. Velocity of DNA during translocation through a solid-state nanopore. Nano Lett. 2015;15(1):732–7. https://doi.org/10.1021/nl504375c.
37. Chen K, Jou I, Ermann N, et al. Dynamics of driven polymer transport through a nanopore. Nat Phys. 2021;17:1043–9. https://doi.org/10.1038/s41567-021-01268-2.
38. Mihovilovic M, Hagerty N, Stein D. Statistics of DNA capture by a solid-state nanopore. Phys Rev Lett. 2013;110(2):028102. https://doi.org/10.1103/PhysRevLett.110.028102.
39. Raper AT, Stephenson AA, Suo Z. Functional insights revealed by the kinetic mechanism of CRISPR/Cas9. J Am Chem Soc. 2018;140(8):2971–84. https://doi.org/10.1021/jacs.7b13047.
40. Gong S, Yu HH, Johnson KA, Taylor DW. DNA unwinding is the primary determinant of CRISPR-Cas9 activity. Cell Rep. 2018;22(2):359–71. https://doi.org/10.1016/j.celrep.2017.12.041.

Publisher's note